Title

Residual Stress Measurements in Dissimilar Weld Metal

Journal

Experimental Mechanics, 55(6)

ISSN

0014-4851

Authors

Olson, MD
Hill, MR
Clausen, B
et al.

Publication Date

2015-07-01

DOI

10.1007/s11340-015-0010-8

Peer reviewed

Residual Stress Measurements in Dissimilar Weld Metal

Mitchell D. Olson[1], Michael R. Hill[1*], Bjorn Clausen[2], Michael Steinzig[3], and Thomas M. Holden[4]
[1] *Department of Mechanical and Aerospace Engineering, University of California, One Shields Avenue, Davis, CA 95616*
[2] *Los Alamos Neutron Science Center, Los Alamos National Laboratory, PO Box 1663, Los Alamos, NM 87545*
[3] *Los Alamos National Laboratory, W-2, PO Box 1663, Los Alamos, NM 87545*
[4] *Northern Stress Technologies, Deep River, Ontario, Canada K0J 1P0*

Submitted to *Experimental Mechanics*, November 2014
Accepted in revised form March 2015.
https://doi.org/10.1007/s11340-015-0010-8

ABSTRACT

This paper describes measurements of residual stress in thin slices removed from the wall of a pressurizer safety/relief nozzle, which is a cylindrical welded component found in a nuclear power pressurized water reactor. Because the slices comprise a cross-section through a dissimilar metal weld that joins the low-alloy steel pressurizer to a stainless steel safe-end, the residual stress measurements are difficult. Typical welds have large grains and preferred orientations, along with chemical and phase gradients, that challenge diffraction techniques using neutron or x-ray beams. Welds also contain spatial gradients of residual stress that challenge mechanical release techniques like contour, slitting, and hole drilling. Therefore, the paper describes the application of, and compares the results from, three applicable residual stress measurement techniques: slitting, electronic speckle pattern interferometry hole drilling, and neutron diffraction. The results of slitting and neutron diffraction are in rough agreement, while the results from hole drilling are significantly different. An uncertainty analysis shows that slitting results had the smallest uncertainty, followed by hole drilling, and that neutron diffraction results had large uncertainty, particularly in the weld.

Keywords: Residual stress, welding, slitting, neutron diffraction, hole drilling, electronic speckle pattern interferometry

1. INTRODUCTION

Residual stresses are particularly subtle because they show no external evidence of their existence. The effects of these stresses can be significant in safety critical structures, especially for components that are at risk of long-term degradation due to stress corrosion cracking or fatigue. For stress corrosion cracking, residual stresses can be the sole driving force for crack nucleation and growth, where the material is susceptible and exposed to a corrosive environment. For fatigue, residual stresses contribute

* Corresponding author. Tel.: 530-754-6178; fax: 530-752-4158.
E-mail address: mrhill@ucdavis.edu

to the mean stress, and mean stress intensity factor, and thereby affect the time to crack nucleation and then the rate of crack growth.

Certain welds found in nuclear power pressurized water reactors (PWRs), called “transition” or “dissimilar metal” welds, join stainless steel piping to the nozzles of low-alloy steel pressure vessels, such as the reactor pressure vessel or the pressurizer. To improve weld quality, dissimilar metal welds typically have a weld “butter” applied to the low-alloy steel nozzle, which is usually subject to thermal stress relief. Subsequently, the dissimilar metal weld is made between the butter and either stainless steel piping or, more commonly, a short stainless steel pipe-like stub known as a “safe end”. The weld butter and the dissimilar metal weld are typically made with nickel-based alloys (historically A82/182, but more recently A52/152) that have a coefficient of thermal expansion between those of the low-alloy steel and the stainless steel materials joined together, which helps to alleviate thermo-elastic stress. Operational experience shows A82/182 weld joints to be susceptible to stress corrosion cracking. For example, nearly 1 mm of crack growth per year can occur in a corrosive environment (3.5 ppm lithium, 1800 ppm boron, and 30-35 cc/kg dissolved hydrogen) at a low stress intensity factor (10 MPa $m^{1/2}$) and typical operating temperature (325º C) [1]. Tensile stress fields are required for stress corrosion cracking, and tensile weld residual stresses are considered a significant issue in operational experience [2].

Knowledge of residual stress in nickel alloy welds is fundamental to managing risk of stress corrosion cracking in nuclear power plants. Currently, the most developed method of mapping the axial and hoop stress in the vicinity of a cylindrical weld is neutron diffraction. However, typical nozzles are welded and have thicknesses of 25.4 to 76.2 mm (1 to 3 inch), which makes measurements with neutron diffraction difficult due to long path lengths, high neutron attenuation, large grain sizes in the weld, and crystallographic texture. These difficulties were demonstrated in a recent neutron diffraction study

performed by Brown et al. [3], which was carried out on the same nozzle studied here, with this work using a thin slice cut from the nozzle wall, but the work of Brown et al. using the entire nozzle. Despite cutting a "window" in the nozzle, to shorten the effective neutron path length, the diffraction measurements remained difficult, and only qualitative results were obtained. The measurements showed tensile hoop strain in the weld region (indicating tensile hoop stress), but stress could not be computed because it was not possible to determine axial strain conclusively. Given the findings of that work, the authors have been engaged in the development of different measurement approaches for large nickel based welds typical of nuclear power plants.

The primary purpose of this work is to compare in-plane residual stress maps formed using different measurement techniques in a welded component with the complicated material condition typical of dissimilar metal welds. However, this work also addresses one of the key steps in a new stress mapping approach for large cylindrical nozzles recently described by Hill and Olson [4]. This new approach uses a superposition of results from multiple measurement techniques to provide a two-dimensional map of biaxial (hoop and axial) stresses through the wall thickness of a cylindrical body, and builds upon earlier work by Pagliaro, Prime, et al. [5], which used a disc geometry. In this new approach, hoop stress is measured using the contour method, and then subsequent measurements are made of the axial stress remaining in thin slices removed adjacent to the contour plane. The data from these two sets of measurements provide a map of the hoop and axial stress when supplemented by a finite element computation that determines the axial stress released when slices are removed from the nozzle [4]. One advantage of this approach is that the axial stress field in the thin slice can be measured by a number of techniques. In particular, neutron diffraction measurements have a much shorter path length in a thin slice than in the original cylinder, which would enable more precise stress mapping. The work reported here comprises the application of different residual stress measurement techniques to determine the

distribution of axial residual stress in a set of slices removed from the wall of a PWR nozzle, enabling a comparison of results from each technique.

Three techniques were selected to measure residual stress in the thin slices. The three techniques are neutron diffraction (ND), slitting (earlier known as the crack compliance method), and electronic speckle pattern interferometry (ESPI) hole drilling. The three techniques differ in several regards, including the components of the stress tensor they determine and the spatial volume over which they determine (i.e., average) residual stress. All three techniques were used to map axial stress as a function of the axial and radial position in the slice. The ND and ESPI hole drilling techniques also determined the radial residual stress, but because radial residual stresses have never been shown to drive material degradation in PWR welds, only axial stresses are considered here. These three measurement techniques were selected because of their applicability to stress mapping in the slice geometry, anticipated precision, and widespread use. Results of this technique comparison will inform future biaxial stress mapping measurements.

2. METHODS

Several slices were removed from a welded PWR pressurizer safety and relief nozzle that had been acquired from a cancelled nuclear power plant. The nozzle has a girth weld in a single V configuration with the weld butter having approximately 50 passes and the dissimilar metal weld having approximately 9 passes. The full nozzle is 375 mm (14.75 inch) long, with a 203.2 mm (8 inch) outer diameter and 35 mm (1.378 inch) wall thickness (Fig. 1a). Slices were removed along radial-axial planes, and each slice had a hoop-direction thickness of 5 mm (0.20 inch) at mid-wall. Slices were cut using a wire electric discharge machine (EDM). The slice used for ESPI hole drilling measurements was electropolished to remove the EDM recast layer that could affect surface residual stress measurements [6]. The pressure vessel side of the nozzle is low-alloy steel (SA-508 Gr2), while the piping side of the

nozzle and the cladding are stainless steel (316 SS). Both the weld and weld butter are made of nickel based weld filler metal (Alloy 182 for the butter and Alloy 82/182 for the weld) (Fig. 1b). The coordinate system in Fig. 1b will be used throughout this paper, where the origin is at the center of the weld at the ID with the positive *x*-axis toward the low-alloy steel side and the positive *r*-axis toward the OD. The material mechanical properties used are given in Table 1 [7].

Measurements were made at locations optimized with respect to each technique. For neutron diffraction, the measurements have high spatial density (possible since the count times were relatively low in the thin slice), and used a cubic gage volume with side length of 2 mm. Since EPSI hole drilling and slitting are mechanical release measurement methods, it is important to space the measurements far enough away from previous measurement locations, so that the previous measurements have an effect on future measurements that is either negligible or correctable. Three slices were used for the slitting measurements. For two of the three, the distance between measurement planes was 20 mm and for the third slice it was 10 mm (Fig. 2). For the second and third measurements on a given slice, a correction was needed to account for the stress that was released from previous measurements. The correction was found using a supplemental elastic stress analysis, following earlier work [8]. The supplemental analysis used stress found in the prior measurement as an input traction boundary condition, applied at the prior measurement plane, to determine the stress induced by that traction at the subsequent measurement plane, which comprises the correction. For ESPI hole drilling, the measurement locations were performed in a grid with distance between measurement sites of five times the hole diameter, which was 1.6 mm, so that there would be negligible effects from adjacent measurements. It should be noted at this point that if the full nozzle is axisymmetric, then the stress in each slice would be the same, as confirmed by an earlier numerical experiment [4]. By assuming axisymmetry, measurements from separate slices can be compared, as if they were performed on a single plane. In addition, these thin

slices are expected to have minimal in-plane stress variation through the thickness, so single increment hole drilling was performed.

The neutron diffraction results were processed using standard methods [9] by collecting lattice spacing (*a*-spacing) in a slice containing residual stress, as well as the lattice spacing in a stress-free sample (a_0-spacing) for three orthogonal strain components. The neutron diffraction measurements were made at SMARTS [10] in the Los Alamos Neutron Science Center (LANSCE). SMARTS is a time-of-flight instrument with two detector banks at ±90º from the incident neutron beam that allow two orthogonal lattice spacings to be measured simultaneously. The lattice spacings were found using the full diffraction pattern with GSAS [11]. A stress-free (a_0) sample was made by cutting many "teeth" into an available slice using wire electric discharge machining (EDM) (Fig. 3). The assumption is made that the chemical composition at each position is identical in the two slices, which may not be correct since alloying, and alloy boundaries can vary around the tube. Each normal component of the residual strain tensor is typically found from the lattice spacing as

$$\varepsilon_i = \frac{a_i - a_{0,i}}{a_{0,i}} \tag{1}$$

where ε_i is strain and $i = x$, r, or h to denote the axial, radial, or hoop component. It is also crucial to measure the component of strain in the reference and the intact sample in the same bank. This is because the value of the lattice spacing is significantly different in the two banks even when the equipment is calibrated with a standard powder. This originates in the wavelength and intensity differences in the white beam spectrum across the neutron beam. The normal components of the residual stress tensor are computed with Hooke's law [12]

$$\sigma_i = \frac{E}{1+\nu}\left(\varepsilon_i + \frac{\nu}{1-2\nu}\left(\varepsilon_x + \varepsilon_r + \varepsilon_h\right)\right) \tag{2}$$

for i =r, x, or h, where E is the elastic modulus and ν is Poisson's ratio. Since the present part is a thin plate, the stress state can be assumed to be plane stress ($\sigma_h = 0$). This assumption allows the a_0-spacing at each measurement point in the intact sample to be calculated as [13]

$$a_{0,p\sigma} = \frac{1-\nu}{1+\nu} a_h + \frac{\nu}{1+\nu}\left(a_x + a_r\right) \tag{3}$$

where $a_{0,p\sigma}$ is the stress-free lattice spacing using the plane stress assumption. This has the advantage that the lattice spacing is obtained in the intact sample not in a second plate. In addition, an estimate of normal stresses can then be found using the plane stress assumption and the derived $a_{0,p\sigma}$ spacing in Eq. (3), namely

$$\sigma_i = \frac{E\left(a_i - a_h\right)}{a_h + \nu\left(a_x + a_r - a_h\right)} \tag{4}$$

for i =r, x. However, this also requires that the values of the measured spacings be corrected for the bank differences referred to above. The ratio between the banks was obtained from reference measurements made far from the weld in both the low alloy steel and the stainless steel. There was no through-wall variation of the measured lattice parameter in either material. Neither was there an indication of errors originating in large grain effects since the errors for both materials in the average lattice parameter were the same and consistent with the uncertainties derived from the Rietveld fitting process. The bank1/bank2 ratios from the ferritic and austenitic steels were 0.99972±0.00013 and 0.99983±0.00015 and the average value was taken to put all the measured lattice spacing data on a common scale. The uncertainty for the neutron diffraction measurements was computed using only the root mean deviation assigned by the Rietveld fitting using GSAS, which will be called the misfit. This misfit was used as the uncertainty in lattice spacing and propagated through the above equations for strain and stress [14] to find the total uncertainty, u, for each stress component from

$$u^2 = \sum_i^N \left(\frac{\partial f}{\partial x_i} \right) u_{x_i}^2 \quad (5)$$

where f is the equation relating measured independent variable x_i having uncertainty u_{xi}, and N is the number of independent variables in f. Data analysis showed lower uncertainty for the plane stress derived stresses of Eq. (4), than those derived from the standard approach because only one difference appears in Eq. (4) whereas three differences in lattice parameter are combined in Eq. (2). The plane-stress stresses are used to present the neutron diffraction results below; however, a comparison of strains and stresses computed using the two different stress-free lattice spacing definitions is discussed later. Where large grains do affect the results, in the weld metal and heat-affected zones the scatter from point-to-point, which gives a measure of the accuracy, is much larger than the Rietveld misfit, which is more akin to a precision since it estimates the effects of random uncertainties on the measurement.

Slitting uses material removal to cause deformation, which is then used to calculate residual stress, as typical of all mechanical release methods [15]. For slitting, a strain gage is placed on the back face of a sample being cut and strain is recorded for a series of cut depths. The stress is then found by solving an inverse problem relating the measured strain to the best fit stress using a "compliance" matrix [15]. The compliance matrix is the strain that would be caused by a unit stress applied to each cut increment at each cut depth, which forms a lower triangular matrix. The computation of the compliance matrix was preformed using a 2D finite element analysis [16] with a variable thickness beam assumption [17]. The 2D simulation was verified to be accurate using a full 3D analysis where the slice had a tapered cross section.

Experimental details for slitting followed typical procedures [18]. The slit was cut with a wire EDM using 250 μm (0.010 inch) diameter brass wire. A strain gage with a length of 0.82 mm (0.032 inch) was applied to the back face of the slitting measurement plane (OD side of slice) using typical strain gage application procedures, after which the gage was waterproofed. The maximum slit depth was nominally

30 mm (about 90% of the slice radial thickness). The regularized unit pulse method with Tikhonov regulation [19] was used to compute stress from the measured strain. The regularization penalizes the second derivative of the stress, which provides useful smoothing. The uncertainties in the slitting results were found using the methods developed by Prime and Hill [20]. In this case, since regularized unit pulses were used as the basis, the model error term was excluded and only the strain measurement uncertainty term was used, taken as the maximum of either the misfit between measured strain and fitted strain, or a minimum value of 2 με.

Similar to slitting, ESPI hole drilling uses the deformation caused by material removal (drilling a hole) and an analysis routine to calculate residual stresses. The specimen was securely clamped and a hole was drilled using a high-speed drill, then deformation around the hole was determined. Near-hole deformation was measured using ESPI, which uses a single coherent light source that is split, part of the split beam used to illuminate the object, called the object light, and part used as reference light. The reference light is interfered with the object light, and an interference image, called an interferogram, is recorded with a CCD camera both before and after the hole is drilled. Deformation around the hole causes the path length of the object light to change, which causes a shift in phase [21]. The phase shift between before and after images provides the spatial deformation field around the hole. To compute residual stress, ESPI hole drilling requires an equivalent to the compliance matrix used in slitting. Specifically, a series of models of holes with applied stresses were developed and resulting deformations form a look-up table to match measured deformations to residual stresses.

ESPI hole drilling measurements were made at Los Alamos National Laboratory, at LANSCE, using typical methods, similar to those described in [22]. The hole drilling was performed with a commercial ESPI hole drilling system (PRISM [23]), which consisted of a high-speed drill, a laser light source, and a CCD camera. The drill remained at a fixed height, so the sample was positioned using a fixture that

allowed the drill to reach each measurement point. The fixture was clamped to an air table and consisted of a backing plate with slots that supported the slice (to adjust its vertical position); the slice was then clamped to the backing plate. The hole drilling equipment and fixture are shown in Fig. 4. The drill bit diameter was 1.6 mm, the hole depth was 0.30 mm (single increment), and the drill speed was 20,000 rpm. The PRISM software calculates residual stress using the methods like those described by Schajer [24]. Several interference images were taken after each hole was drilled, allowing the residual stress to be calculated several times for each hole. Using the repeated stress measurements, the uncertainty was calculated using a statistical analysis [14]

$$u = \pm \frac{t_{N,c}}{\sqrt{N}} std(\sigma)$$
$$std(\sigma) = \sqrt{\frac{1}{N-1}\sum_{i=1}^{N}(\sigma_i - \sigma_{mean})^2} \quad (6)$$

where u is the uncertainty, N is number of measurements, c is the confidence interval, and $t_{N,c}$ is the range of Student's t distribution corresponding to a given N and c, $std(\sigma)$ is the standard deviation, and σ_{mean} is the mean of the measurements. For these measurements, we used $N = 5$ and $c = 95\%$.

For comparison with the measured residual stress maps, we developed an estimate of residual stress in the removed slice using an axisymmetric finite element welding simulation. The model assumed a representative geometry, being 362 mm (14.25 inch) long with a 132 mm (5.2 inch) inner diameter and a 35 mm (1.378 inch) wall thickness. The simulation consisted of two sequentially-coupled analysis steps, the first thermal and the second thermo-mechanical, conducted in commercial finite element software [16]. The axisymmetric mesh contained 4,041 finite elements, where 8-node quadratic interpolation heat transfer axisymmetric elements (DCAX8) were used in the thermal analysis and 8-node reduced integration quadratic interpolation axisymmetric elements (CAX8R) were used in the mechanical analysis. The node spacing was small near the weld (around 1 mm) and larger away from the weld. All

materials used the temperature-dependent thermo-physical and thermo-mechanical material properties given in [7]. The resulting pass-by-pass temperature history calculated in the thermal analysis was used as input for a subsequent thermo-mechanical analysis. The thermo-mechanical analysis used a temperature dependent isotropic hardening model. Further details on the simulation can be found in a paper from Fredette et al. [25].

The results of the axisymmetric model were used to find the stress that would be present in a three-dimensional slice. The three-dimensional finite element model of the slice was created by revolving the original two-dimensional, axisymmetric weld-simulation model about an axial line of symmetry, replicating the original stresses along specified radial-axial planes, and then allowing the model to come to mechanical equilibrium. Because the slice is thin, the residual stress state in the slice is nearly one of plane stress, but this is not assumed in the three-dimensional analysis. Calculation of stress in the slice was made easier by using an available capability in the commercial software (called symmetric model generation) [16].

3. RESULTS

Fundamental measurement data for each of the three residual stress measurement techniques facilitates understanding of each technique. The full diffraction pattern for a representative point near the weld/weld butter interface from neutron diffraction can be seen in Fig. 5. The plot shows significant measurement signal above background noise, and a good quality fit to the diffraction pattern from GSAS, which was used for data reduction. Similar patterns were obtained at this location, and at a set of other locations, with the part in two orthogonal orientations relative to the beam and neutron detectors.

Strains measured during slitting slice 3 at x = -5 mm are shown in Fig. 6(a). The measured strain has a typical profile, with small measured strains for the initial cuts and larger measured strains as the cut tip approaches the back-face strain gage location. Residual stress determined from the measured strain is

shown in Fig. 6(b), along with the correction for a previous measurement at x = +5 mm and the total stress, with is the sum of the measured stress and the correction. Slice 3 had measurement plane spacing of 10 mm and the correction is quite small (< 10 MPa); measurements on slices 1 and 2 had measurement plane spacing of 20 mm, and with that spacing, the prior-measurement corrections were negligible (i.e., < 1 MPa).

An interferogram from ESPI hole drilling is shown in Fig. 7 for a typical post-hole measurement. The interference fringes show the change in phase around the hole (with the distance between light and dark fringes being half the wavelength of the light source). The interferogram is typical for ESPI hole drilling, with fringe spacing smaller near the hole, where there is larger strain, and larger away from the hole, where there is smaller strain.

The measurement points for all techniques are shown together in Fig. 8. While it was not possible to make measurements with all techniques at identical locations, at the weld center (x = 0 mm), all three techniques have measurement points nearby, allowing comparison on that line with some in-plane spatial interpolation of results (Fig. 9). A comparison can be made on a horizontal line near the mid-thickness (r = 17 mm, Fig. 10a) with no interpolation, but since the stresses there are relatively small, a comparison is also made on a line further toward the OD (r = 21 mm, Fig. 10b) where stresses are larger, but does require interpolate of the ESPI results.

The line plots show there is some agreement among results from all three methods and between the measurement data and the weld simulation output. Along the vertical direction (at the weld center), neutron diffraction, slitting, and the finite element simulation show an oscillating stress profile through the thickness, with tensile stress near the ID and compressive stress near r = 10 mm, back to tensile stress at the OD, whereas the ESPI hole drilling results show higher stress at the ID falling to a smaller stress at the OD, and the final neutron diffraction point measured compressive stress (-100 MPa). Along

the horizontal direction (at r = 17 mm) all three methods and the finite element simulation indicate there are low stresses in the stainless steel, tensile stresses between 25 and 150 MPa in the weld that peak near the weld/butter interface (however, two neutron diffraction measurements found compressive stress in the weld), and lower stresses in the low-alloy steel. Similar trends are seen along the horizontal direction at r = 21 mm, but on this line there is an outlier in the neutron diffraction results at x = 14 mm, and some of the ESPI results have large uncertainty. All of the line plots show a significant difference in uncertainty for the three techniques, with slitting having the lowest uncertainty, ESPI hole drilling having larger uncertainty, and neuron diffraction uncertainty being somewhat larger.

The residual stress maps found with each technique are shown in the left column of Fig. 11, with uncertainty shown in the right column and discussed below. The stress found with neutron diffraction, computed using Eq. (4), has an oscillating stress profile through the thickness near the interface between the weld and weld butter with roughly 100 MPa tensile stress at r = 25 mm and roughly -100 MPa compressive stress at r = 10 mm (this is similar to the trend in the vertical line plot). The slitting results also show an oscillating profile near the interface between the weld and weld butter, with roughly 100 MPa tensile stress at x = 5 and r = 20 mm and roughly -100 MPa compressive stress at x = 5 and r = 10 mm. The stress map from slitting is relatively smooth, without abrupt changes of stress near material interfaces. ESPI hole drilling results exhibit relatively constant stress of 50 MPa over much of the cross section, but with an oscillating stress profile through thickness in the weld butter, similar to that found with neutron diffraction and slitting. The ESPI hole drilling result at x = -25 mm and r = 22 mm appears spurious. The finite element results also show an oscillating profile through the thickness at the weld center, with roughly 170 MPa tensile stress at x = 0 and r = 0 mm, roughly -85 MPa compressive stress at x = 5 and r = 10 mm, and roughly 85 MPa compressive stress at x = 5 and r = 21 mm.

Generally, there is agreement between measurement techniques, with some areas of notable agreement or disagreement. The stresses found with both neutron diffraction and slitting show an oscillating stress profile with position through thickness throughout the weld and weld butter, where there is tensile stress near the ID and near r = 20 mm, and compressive stress near r = 10 mm and near the OD. The ESPI hole drilling results show similar trends compared to the slitting results near the ID, weld butter, and stainless steel cladding, but they do not show the strongly banded structure revealed by the other two techniques. Qualitatively, it appears that neutron diffraction and slitting results are in reasonable agreement with each other and with the finite element simulation, whereas the ESPI hole drilling results differ.

The uncertainty for each measurement technique is significantly different and can be seen in the right column of Fig. 11. The neutron diffraction uncertainty is reasonable over the entire slice, but significantly smaller away from the weld and weld butter (around 20 MPa), and large in the weld and weld butter (around 40 MPa). The uncertainty for the slitting measurements is under 15 MPa for all but one measurement plane, for which there was an experimental issue that resulted in high uncertainty near the OD at x = 5 mm. The uncertainty for the ESPI hole drilling results is under 25 MPa in the mid-thickness, but there are three measurement points with large uncertainty (>150 MPa).

4. DISCUSSION

Overall, the qualitative agreement of the oscillatory through-thickness stress profile near the weld center found with neutron diffraction and slitting, and shown in the weld simulation output, is promising, and gives some confidence in the measurement techniques; however, the ESPI hole drilling results differ significantly from results of the other two techniques. The finite element simulation provided full field stress data through the slice, which was used to test our assumption that there would be limited variation in stress through the slice thickness; such a variation would lead to bias in EPSI hole

drilling, which is a surface measurement technique, relative to ND and slitting, which are thickness-average techniques. The difference between the axial stress at the slice face and the thickness-average axial stress can be seen in Fig. 14, where the thickness-average stress was computed from the three-dimensional slice model output. The stress differences are rather small, except in two areas: one near the ID at the weld center, and one near the interface between the weld butter and the low-alloy steel. These areas of larger difference are near corresponding areas of sharp gradients in elastic properties. While the differences between surface and thickness average stress suggest some bias of ESPI hole drilling relative to ND and slitting, the bias is less than 10 MPa at most locations, which does not explain the differences between results from ESPI hole drilling and the other techniques (e.g., as shown in Fig. 9).

Some aspects of the neutron diffraction results are interesting. Measurements were made near the interface between the weld butter and low-alloy steel, but the results appeared to be spurious, with implausibly large stress (>800 MPa), and were omitted. We suspect errors are related to issues regarding grain size, texture, and multiple phases in that region. Large grain size and texture in the weld and weld butter is a likely cause of the larger uncertainties in the weld region. Neutron diffraction results developed using standard neutron diffraction procedures (i.e. using both the a and a_0 lattice spacing measurements, and Eqs. (1) and (2)), gave large stresses (>400 MPa) in the hoop direction, which are unlikely in such a thin specimen. The plots in Fig. 12 show the difference between measured stress-free lattice spacings and the calculated (plane stress) lattice spacing. Since the material has a cubic lattice, the a_0 in all three orientations are expected to be the same, but were found to be significantly scattered and different. The calculated plane stress a_0 seems reasonable, generally falling between the three measured values, which can be seen in Fig. 12. The differences for the two data processing approaches are shown in Fig. 13 at the weld center for axial strain and axial stress. The results found with the plane stress assumption exhibit a smoother profile, and near the ID and OD change the sign of the stress.

It is interesting that the EPSI hole drilling results have quite good agreement with the weld simulation output at r = 17 mm (Fig. 10a), whereas over the whole cross-section there is limited agreement. Results from ESPI hole drilling compare reasonably well to the other two techniques, at r = 17 mm and 21 mm, but are significantly different at x = 0. One possible reason for the discrepancy at x = 0 is because the comparison is made by interpolating the results in an area without a significant number of measurements. Another possible explanation for the discrepancies is problems with secure clamping during the drilling at some locations. If clamping is not secure, the slice could move during drilling, causing difficulties in data processing and correlation of the images taken before and after drilling. This is a likely cause of the large uncertainties at three of the measurement points. It bears noting that the major advantage of ESPI hole drilling over conventional (strain gage) hole drilling is the speed of measurement, which allowed the large number of measurements required for this study in a reasonable amount of time, but perhaps with some loss of precision.

5. SUMMARY/CONCLUSIONS

Stress measurements were made in slices removed from a pressurizer safety/relief nozzle that contained a dissimilar metal weld. The measurements were made with three techniques, and show the axial stress to have a banded stress profile, with tensile stresses of 100 MPa near the slice ID and near 20 mm from the ID, and compressive stresses of -150 MPa near 10 mm from the ID and near the slice OD. The stresses from neutron diffraction and slitting are in general agreement, and agree well with a finite element simulation, but results from ESPI hole drilling did not show some of the same trends. The uncertainty of slitting results was excellent with most measurements having uncertainty under 15 MPa, which is typical of the technique [26]. Uncertainties for neutron diffraction and ESPI hole drilling results were higher on average, with both having some measurement points with very large uncertainties (>150 MPa). The comparison of the three measurement techniques shows that it is possible to measure in-plane residual stresses with any of the three, but slitting appears to be the best suited measurement technique

since it is insensitive to microstructural issues, provides excellent measurement precision, and can be performed using conventional equipment.

6. ACKNOWLEDGEMENTS

The Electric Power Research Institute, Materials Reliability Program (Paul Crooker, Principal Technical Leader) provided financial support for this work. The PWR nozzle was part of an NRC/EPRI cooperative activity on weld residual stress, and the cooperation of the NRC is appreciated (Aladar Csontos, Matthew Kerr, David Rudland, and Howard Rathbun). During the work, the first author (Olson) was supported by the Los Alamos National Laboratory (LANL) Summer Program (Michael B. Prime, mentor). The neutron diffraction work was funded by grant #20111200 for beamtime at the SMARTS diffractometer at LANSCE. The authors also acknowledge Adrian DeWald (Hill Engineering, LLC) for a portion of the slitting measurements, and Michael B. Prime of LANL for helpful discussions.

REFERENCES

[1] EPRI, "Material Reliability Program Crack Growth Rates for Evaluating Primary Water Stress Corrosion Cracking (PWSCC) of Alloy 82, 182, and 132 Welds", MRP-115NP, Electric Power Research Institute, 2004.

[2] P. Dong and F. Brust, "Welding residual stresses and effects on fracture in pressure vessel and piping components: a millennium review and beyond", *Journal of Pressure Vessel Technology,* vol. 122, pp. 329-338, 2000.

[3] D. W. Brown, T. Sisneros, and T. M. Holden, "Report on residual stress measuremetns by neutron diffraction on a retired safety nozzle from the St. Lucie nuclear power station", *Internal Los Alamos National Laboratory Report,* 2009.

[4] M. R. Hill and M. D. Olson, "Biaxial Residual Stress Mapping in a PWR Dissimilar Metal Weld", PVP2013-97246, ASME 2013 Pressure Vessels & Piping Division Conference, Paris, France, 2013.

[5] P. Pagliaro, M. B. Prime, J. S. Robinson, B. Clausen, H. Swenson, M. Steinzig*, et al.*, "Measuring Inaccessible Residual Stresses Using Multiple Methods and Superposition", *Experimental Mechanics,* vol. 51, pp. 1123-1134, 2010.

[6] W. Cheng, I. Finnie, M. Gremaud, and M. B. Prime, "Measurement of Near Surface Residual Stresses using Electric Discharge Wire Machining", *Journal of engineering materials and technology,* vol. 116, pp. 1-7, 1994.

[7] EPRI, "Materials Reliability Program: Finite-Element Model Validation for Dissimilar Metal Butt-Welds", MRP-316, Electric Power Research Institute, 2011.

[8] W. Wong and M. R. Hill, "Superposition and Destructive Residual Stress Measurements", *Experimental Mechanics,* vol. 53, pp. 339-344, 2013.

[9] ISO, "Non-destructive testing - Standard test method for determining residual stresses by neutron diffraction", ISO/TS 21432, International Organization for Standardization, 2005.

[10] M. A. M. Bourke, D. C. Dunand, and E. Ustundag, "SMARTS - a spectrometer for strain measurement in engineering materials", *Applied Physics A: Materials Science & Processing,* vol. 74, pp. s1707-s1709, 2002.

[11] A. C. Larson and R. B. Von Dreele, "General Structural Analysis System (GSAS)", *Los Alamos National Laboratory Report LAUR 86-748,* 2004.

[12] M. T. Hutchings, P. J. Withers, T. M. Holden, and T. Lorentzen, "*Introduction to the Characterization of Residual Stress by Neutron Diffraction*", Boca Raton, FL, CRC Press, 2005.

[13] P. Staron, M. Koçak, S. Williams, and A. Wescott, "Residual stress in friction stir-welded Al sheets", *Physica B: Condensed Matter,* vol. 350, pp. E491-E493, 2004.

[14] H. W. Coleman and W. G. Steele, *Experimentation, Validation, and Uncertainty Analysis for Engineers*, Ch. 2, John Wiley & Sons, Inc., Hoboken, New Jersey, 2009

[15] M. B. Prime, "Residual stress measurement by successive extension of a slot: The crack compliance method", *Applied Mechanics Review,* vol. 52, pp. 75-96, 1999.

[16] Abaqus/Standard, Version 6.10, Providence, RI, USA, 2010.

[17] E. J. Hearn, "*Mechanics of Materials 1*", Butterworth-Heinemann, 1997.

[18] M. R. Hill, *Practical Residual Stress Measurement Methods*, Ch. 4, John Wiley & Sons, West Sussex, UK, 2013

[19] G. S. Schajer and M. B. Prime, "Use of Inverse Solutions for Residual Stress Measurements", *Journal of Engineering Materials and Technology,* vol. 128, p. 375, 2006.

[20] M. B. Prime and M. R. Hill, "Uncertainty, Model Error, and Order Selection for Series-Expanded, Residual-Stress Inverse Solutions", *Journal of Engineering Materials and Technology,* vol. 128, p. 175, 2006.

[21] M. Steinzig and E. Ponslet, "Residual Stress Measurement using the Hole Drilling Method and Laser Speckle Interferometry: Part I", *Experimental Techniques,* pp. 43-46, 2003.

[22] E. Ponslet and M. Steinzig, "Residual Stress Measurement using the Hole-Drilling Method and Laser Speckle Interferometry Part II: Analysis Technique", *Experimental Techniques,* pp. 17-21, 2003.

[23] "PRISM: Residual stress measurement based on hole-drilling and ESPI", American Stress Technologies, 2000.

[24] G. S. Schajer, "Measurement of Non-Uniform Residual Stresses using the Hole-Drilling Method. Part I - Stress Calculation Proceedures", *Journal of Engineering Materials and Technology,* vol. 110, pp. 338-343, 1988.

[25] L. F. Fredette, J. E. Broussard, M. Kerr, and H. J. Rathbun, "NRC/EPRI Welding Residual Stress Validation Program - Phase III Details and Findings", PVP2011-57645, ASME 2011 Pressure Vessels & Piping Division Conference, Baltimore, MD, USA, 2011.

[26] M. J. Lee and M. R. Hill, "Intralaboratory Repeatability of Residual Stress Determined by the Slitting Method", *Experimental Mechanics,* vol. 47, pp. 745-752, 2007.

TABLES

Material	E (GPa)	ν	Yield Strength (MPa)
316 Stainless steel	195	0.29	562
Alloy 182	210	0.29	693
Low-alloy steel (SA-508, GR2)	207	0.28	590

Table 1: Material mechanical properties (from the ERPI/NRC program on welding residual stress [7])

FIGURES

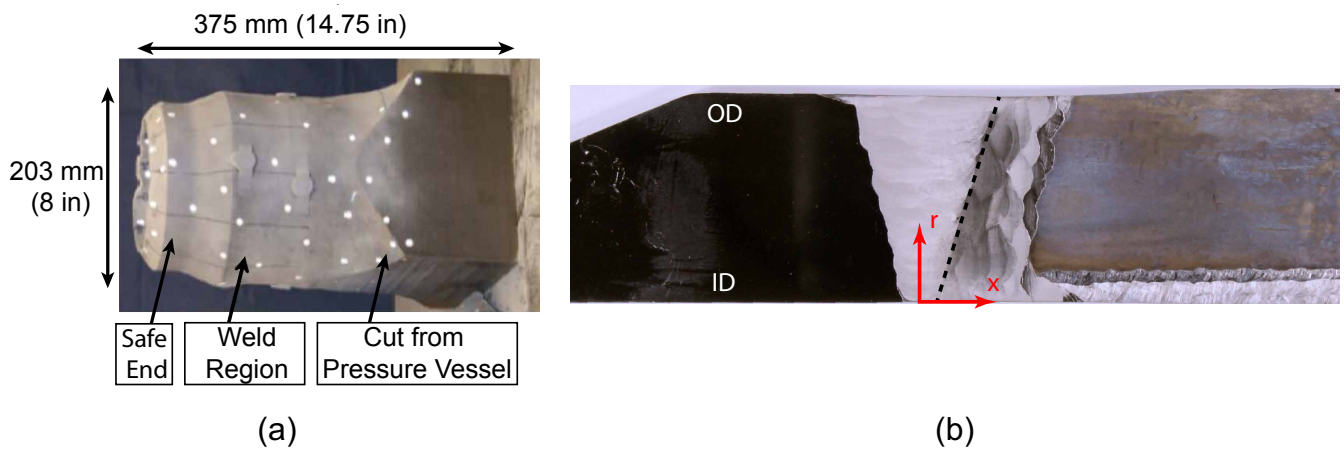

Fig. 1 – (a) Full nozzle geometry and (b) etched nozzle cross-section with coordinate system. The materials in (b) from left to right are stainless steel, Alloy 82/182 weld, Alloy 182 weld butter, and low-alloy steel

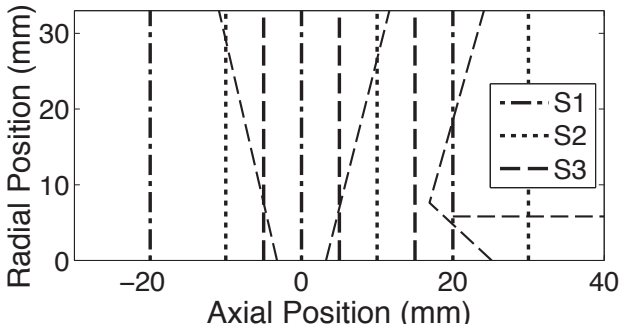

Fig. 2 – Slitting measurement plane used on each of the three slices (slice S1, S2, or S3). The distance between measurement planes for S1 and S2 is 20 mm and for S3 is 10 mm

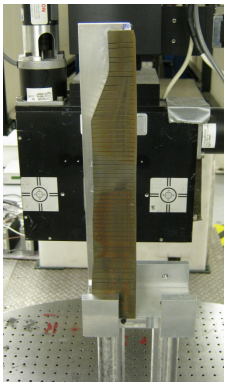

Fig. 3 – Neutron diffraction d_0 sample set-up for measurements in the SMARTS beam line at LANSCE

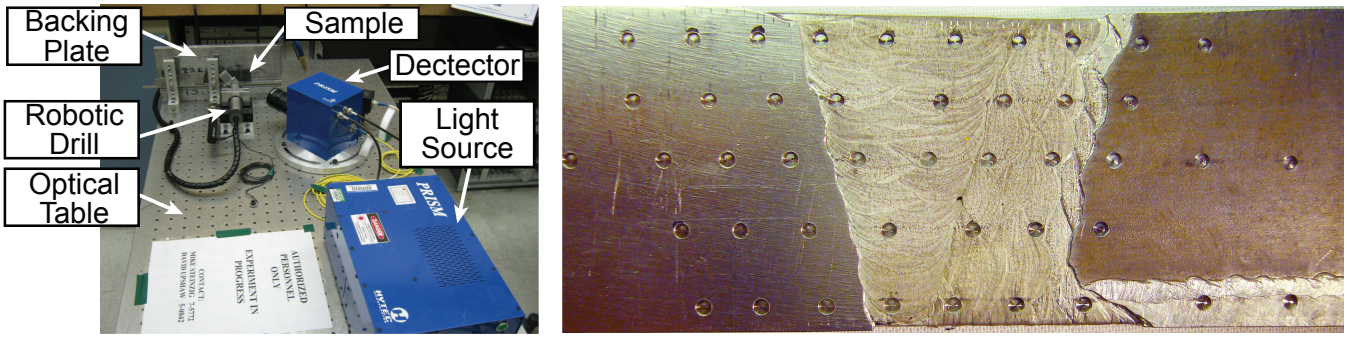

Fig. 4 – (a) EPSI hole drilling experimental set-up and (b) hole drilling locations

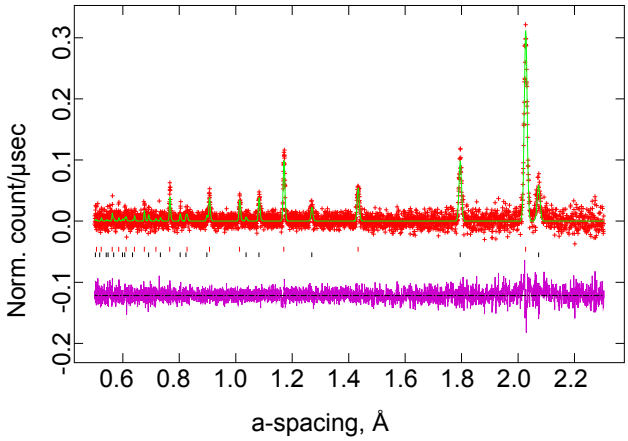

Fig. 5 – Representative neutron diffraction pattern for the stressed (a) sample near the weld/weld butter interface. The plot indicates the number of neutrons diffracted as a function of lattice spacing, indicating the level of scattering relative to background noise

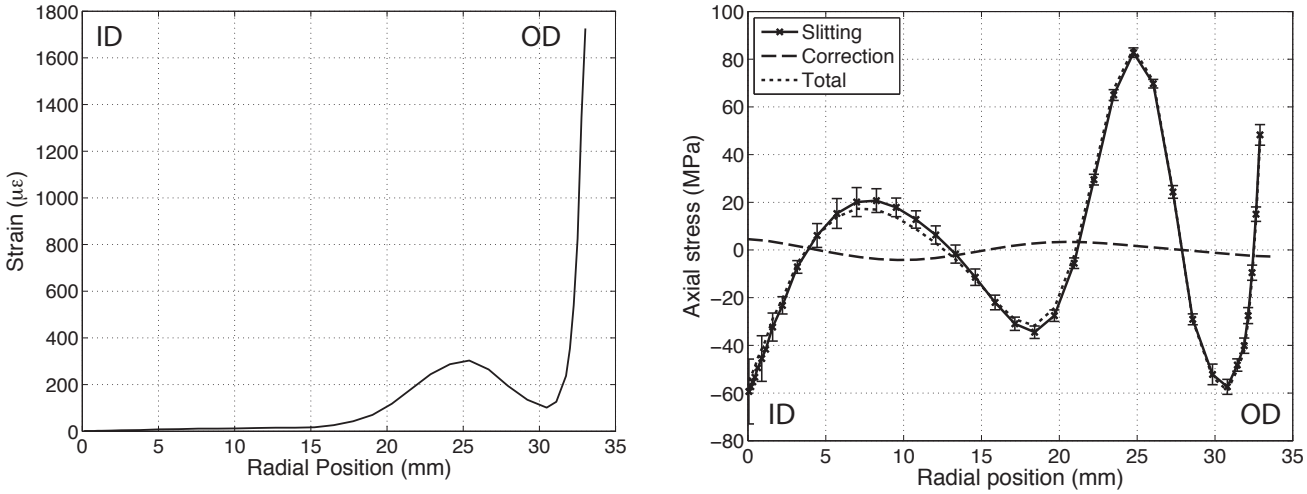

Fig. 6 – Results of slitting slice 3 at the plane x = -5 mm, showing (a) measured strain, and (b) measured residual stress, the correction due to a prior measurement at x = +5 mm, and the sum of the two (i.e., the total stress)

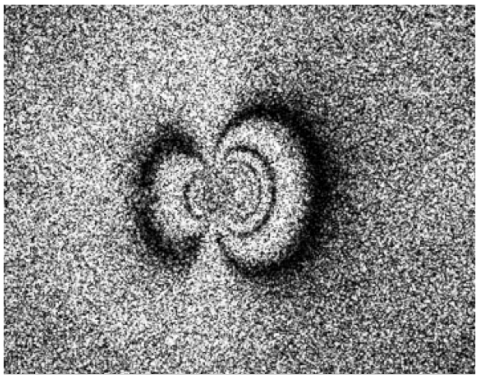

Fig. 7 – Representative interferogram from ESPI hole drilling

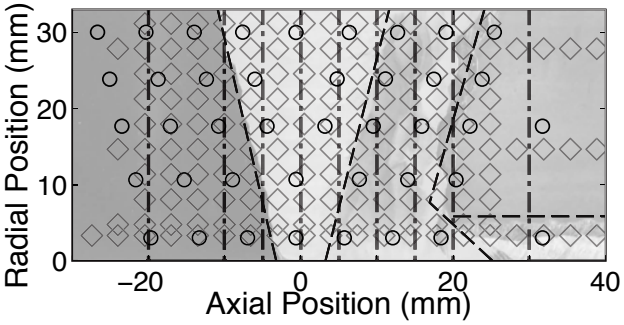

Fig. 8 – Overlapping measurement points from the three techniques. Dash-dotted lines show slitting measurement planes, gray diamonds show neutron diffraction measurement points, and circles show hole drilling locations

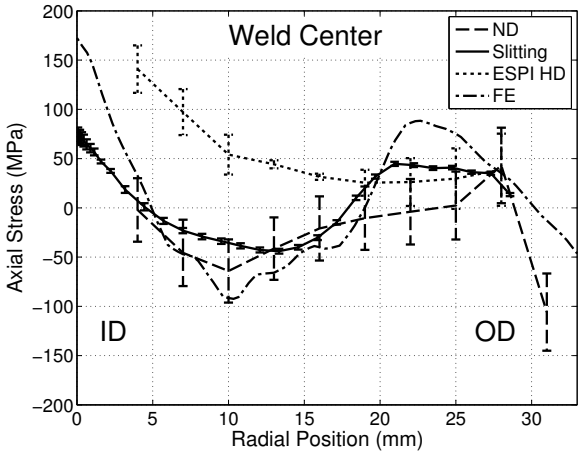

Fig. 9 – Line plot of the axial stress found with each technique, along the radial direction at the weld center

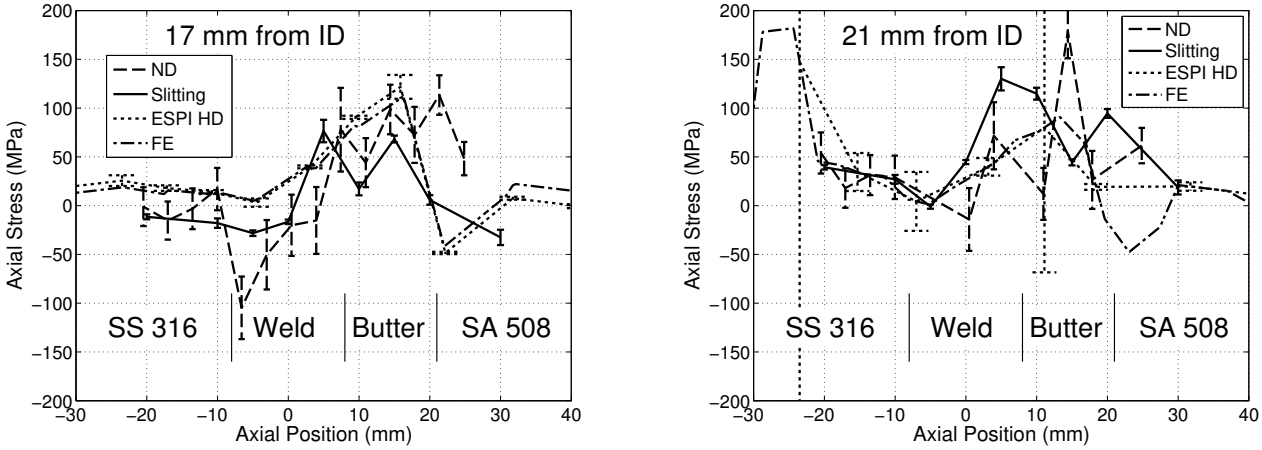

(a) *(b)*

Fig. 10 – Line plots of the axial stress found with each technique, along the axial direction at a radial position of (a) 17 mm from the ID, and (b) 21 mm from the ID

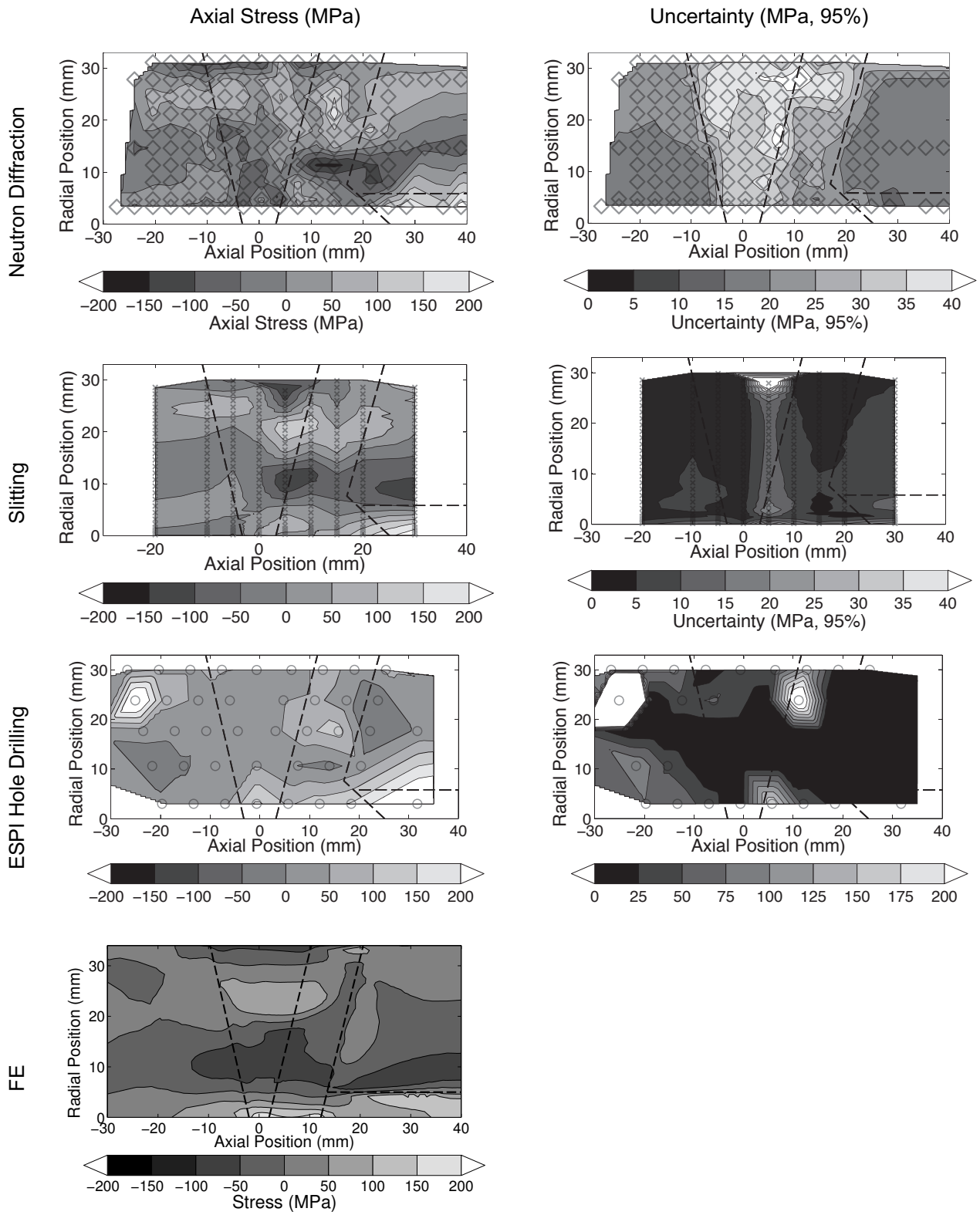

Fig. 11 – Plots of the axial stress (left column) and uncertainty (95% confidence interval, right column) found using neutron diffraction (top row), slitting (second row), ESPI hole drilling (third row), and finite element simulation (FE, bottom row)

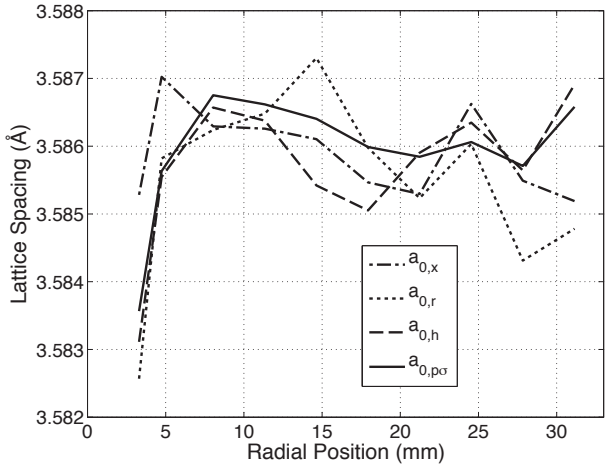

Fig. 12 – Measured neutron diffraction d_0 lattice spacings and calculated plane stress a_0 lattice spacing at the weld center

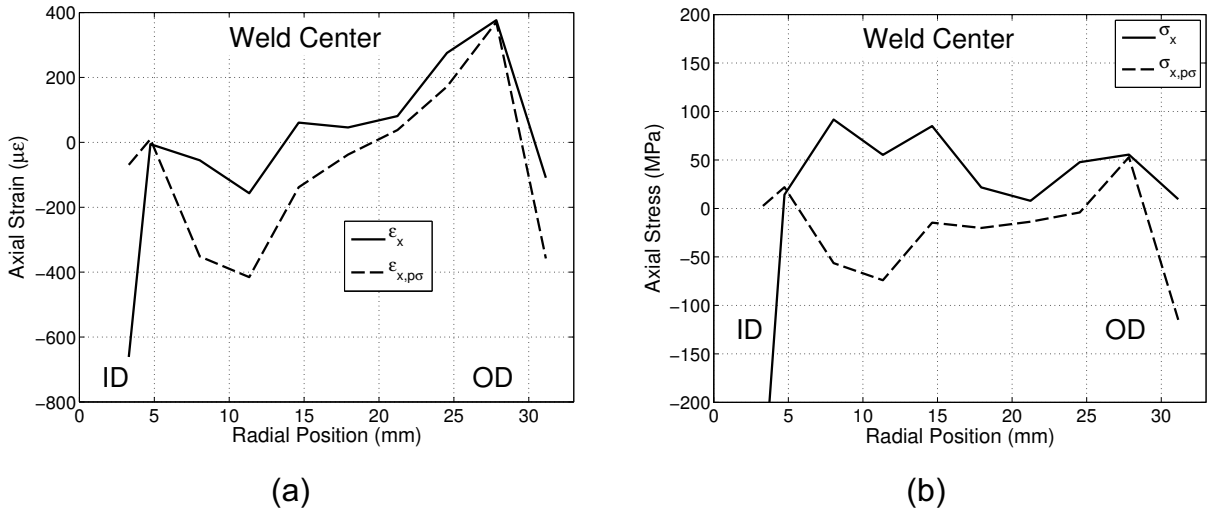

Fig. 13 –Line plots along the radial direction at the weld center for (a) axial strain using measured d_0 lattice spacing and calculated plane stress d_0 lattice spacing and (b) axial stress using measured d_0 lattice spacing and calculated plane stress d_0 lattice spacing at the weld center

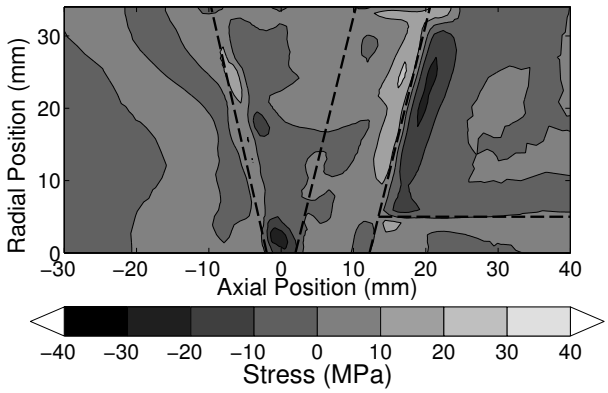

Fig. 14 –Axial stress difference in the finite element simulation between the axial stress at the slice face and the thickness averaged axial stress